JOURNAL OF MATERIALS SCIENCE 23 (1988) 101–110

Aspects of the adhesion and corrosion resistance of polyelectrolyte-chemisorbed zinc phosphate conversion coatings

T. SUGAMA, L. E. KUKACKA, N. CARCIELLO, J. B. WARREN*
*Process Sciences Division and *Instrumentation Division, Department of Applied Science, Brookhaven National Laboratory, Upton, New York 11973, USA*

The ability of polyelectrolyte macromolecules to suppress the crystal growth of zinc phosphate (Zn · Ph) conversion coatings depends primarily on the functional pendant groups. The extent of segmental chemisorption of macromolecules having carboxylic and sulphonic acid groups on the embryonic crystal faces was found to be considerably higher than that of macromolecules containing amine groups. The reaction products formed by intermolecular reactions between amide groups in polyurethane coatings and carboxylic acid groups on the outermost surface of polyelectrolyte-modified Zn · Ph in Zn · Ph-to-polymer adhesive joint systems played an essential role in developing interfacial adhesive forces. A highly dense precipitation of Zn · Ph derived from a zinc orthophosphate dihydrate-based phosphating solution contributed significantly to reducing the corrosion rate of cold-rolled steel. It also was determined that the presence of an internally diffused polyelectrolyte in the Zn · Ph layers further enhances the resistance to corrosion of Zn · Ph itself.

1. Introduction

The internal diffusion and segmental chemisorption of polyacrylic acid (PAA) macromolecules, either on newly precipitated crystal nuclei or on crystal growth sites during primary zinc phosphate (Zn · Ph) conversion processes applied to mild carbon cold-rolled steel surfaces, contribute significantly to the controllability of Zn · Ph crystal dimensions [1, 2]. The composite structure of Zn · Ph chemisorbed with PAA macromolecules of appropriate molecular weight formed a highly dense but fine crystal topography which improved the stiffness and ductility characteristics of the normally brittle Zn · Ph layers [3]. The presence of organic functional groups, such as ionic carboxylate and carboxylic acid, on the outermost surface sites of the chemisorbed crystal layers led to a large increase in the adhesive bonds at the polymer topcoat-to-crystal precoat interfaces [4].

Studies on modifying the material characteristics of Zn · Ph conversion coatings have focused on the inclusion of PAA macromolecules selected from among various polyelectrolytes. However, experimental studies with other polyelectrolytes have not been performed. One of the objectives of this paper is to summarize our findings showing how the functional species of polyelectrolyte macromolecules suppress the crystal growth of Zn · Ph and promote adhesive forces with polymeric topcoatings. The metal substrates used were high strength sheet steels fabricated from low-carbon cold-rolled steel with a carbon concentration of 0.06%. In earlier work, a mild carbon steel (C ~0.23%) was used for the substrate.

Since high strength cold-rolled steels are widely used for automobile body panels to reduce weight, it is very important to determine the ability of polyelectrolyte-modified Zn · Ph coatings to protect them from corrosion by salt solutions from the roads. Hence, the second goal of this investigation was to study the electrochemical behaviour of Zn · Ph coatings derived from a unique zinc orthophosphate dihydrate-based phosphating solution, and to elucidate the effects of the polyelectrolyte when it was internally diffused throughout the crystal layers on the protection afforded by the Zn · Ph layer against corrosion.

2. Experimental procedure

2.1. Materials

The metal substrate used was a high strength cold-rolled sheet steel supplied by the Bethelehem Steel Corporation. The steel contained 0.06 wt % C, 0.6 wt % Mn, 0.6 wt % Si and 0.07 wt % P. The zinc phosphating liquid consisted of 5 parts zinc orthophosphate dihydrate and 95 parts of 10% H_3PO_4, and was modified by incorporating a water-soluble polymer at concentrations ranging from 0 to 4.0% by weight of the total solution. Four polyelectrolytes obtained from Scientific Polymer Products, Inc. were used; polyacrylic acid (PAA; $\{CH_2–CH(COOH)\}_n$), polyitaconic acid (PIA; $\{CH_2C[(COOH)]CH_2OCOH]\}_n$), polystyrenesulphonic acid (PSSA; $\{CH_2–CH(C_6H_4SO_3H)\}_n$), and poly-2-acrylamid-2-methylpropane sulphonic acid (PAMSA; $\{CH_2C[CONH_2C(CH_3)_2CH_2SO_3H\}_n$). For the purpose of comparison with the polyacid macromolecules, two water-soluble polymers were employed, polyacrylamide (PAM; $\{CH_2–CH(CONH_2)\}_n$) and polyvinylpyrolidone (PVP; $\{CH_2–CH(C_3H_5CONH)\}_n$),

0022–2461/88 $03.00 + .12

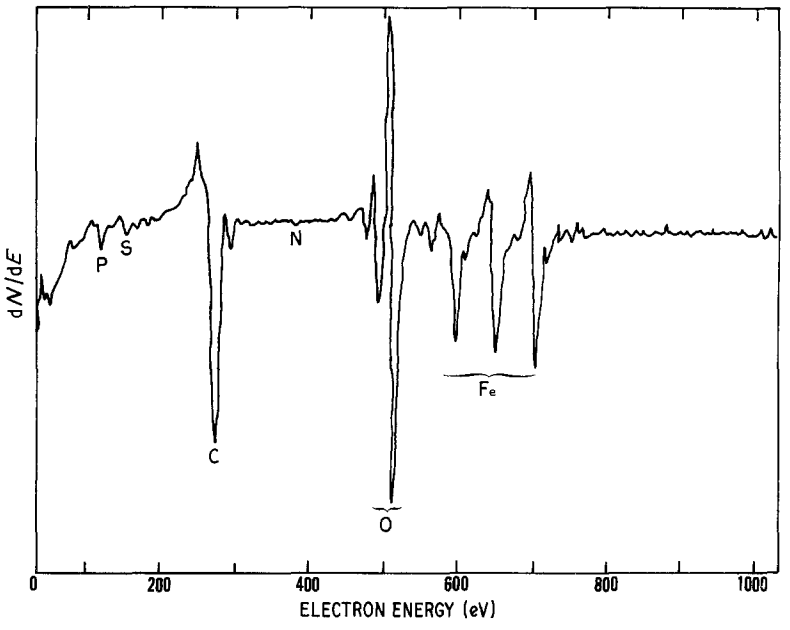

Figure 1 Auger survey spectrum from the solvent-cleaned steel surface. Analysis (%): P2.5, S0.8, C39.5, N2.7, O33.1, Fe21.1.

also from Scientific Polymer Products, Inc. All of these macromolecules, with an average molecular weight in the range of 40 000 to 120 000, were dissolved in water to prepare a 25% polymer solution.

An array of the macromolecule–Zn · Ph composite conversion layers having crystal dimensions of the order of micrometres on the substrate surface was prepared in the following way. The metal substrate was first rinsed with an organic solvent to remove any surface contamination with mill oil. A typical Auger spectrum of the solvent-cleaned steel surface is shown in Fig. 1. The consequent quantitative data indicated that the predominant element at the outermost surface sites of the steel was carbon. Several investigators have reported that the presence of surface carbon impedes the formation of high-quality Zn · Ph coatings [5–7]. Low zinc and phosphorus levels in Zn · Ph deposited on high-carbon areas lead to a porous structure and poor bonding to the steel. These characteristics result in a higher availability of oxygen and moisture at the interface between the Zn · Ph and steel and promote a cathodic delamination reaction. Based upon these features, the quality of the steel surface used in our work upon which the Zn · Ph was deposited can be categorized as inferior.

After rinsing with the organic solvent, the steel was immersed for up to 20 min in the coating solution described above at a temperature of 80° C. Then, it was placed in an oven at 150° C for ~30 min to remove any moisture from the deposited conversion film surface and to solidify the polyelectrolyte macromolecules.

Commercial-grade polyurethane (PU) was applied as an elastomeric topcoating, the polymerization of which was initiated by incorporating a 50% aromatic amino curing agent. The topcoat system was then cured in an oven at a temperature of 80° C.

2.2. Measurements

An image analysis was conducted of the surface microtopography and the surface chemical components of the polyelectrolyte-modified Zn · Ph coatings using an AMR 100 Å scanning electron microscope coupled with a TN-2000 energy-dispersion X-ray spectrometer.

Auger electron spectroscopy (AES) combined with argon ion sputter-etching was used in depth–composition profiling studies to detect interdiffusion of elemental composition at internal interfaces in the polyelectrolyte-adsorbed Zn · Ph layers. A Perkin-Elmer PHI Model 610 scanning Auger microprobe was used.

A Perkin-Elmer Model 257 spectrometer was employed for specular reflectance infrared (IR) spectroscopic analysis. To explore the interfacial interaction mechanisms at the polyelectrolyte-to-polyurethane joints, we recorded IR spectra from thin film samples overlaid on reflecting aluminium mirror surfaces.

Peel strength tests of adhesive bonds at the polyurethane topcoat-modified metal substrate interfaces were conducted at a separation angle of ~ 180° and a crosshead speed of 5 cm min.$^{-1}$ The test specimens consisted of one piece of flexible polyurethane topcoat, 2.5 cm × 30.5 cm, bonded for 15.2 cm at one end to one piece of flexible or rigid substrate material, 2.5 cm × 20.3 cm, with the unbonded portions of each member being face to face. The thickness of the polyurethane topcoat overlaid on the complex crystal surfaces was ~0.95 mm.

The electrochemical testing for data on corrosion was performed with an EG & G Princeton Applied Research Model 362-1 corrosion measurement system. The electrolyte was a 0.5 M sodium chloride solution made from distilled water and reagent-grade salt. The specimen was mounted in a holder and then inserted into an EG & G Model K47 electrochemical cell. The exposed surface area of the samples was 1.0 cm^2. Prior to immersion of the test specimens the solution was de-aerated by bubbling nitrogen through for 30 min. Nitrogen gas then flowed over the top of the NaCl solution containing the specimens for 60 min to stabilize the corrosion potential, before polarization was initiated. The cathodic and anodic polarization curves were determined at a scan rate of 0.5 mV sec^{-1} in the corrosion potential range of −1.2 to −0.2 V.

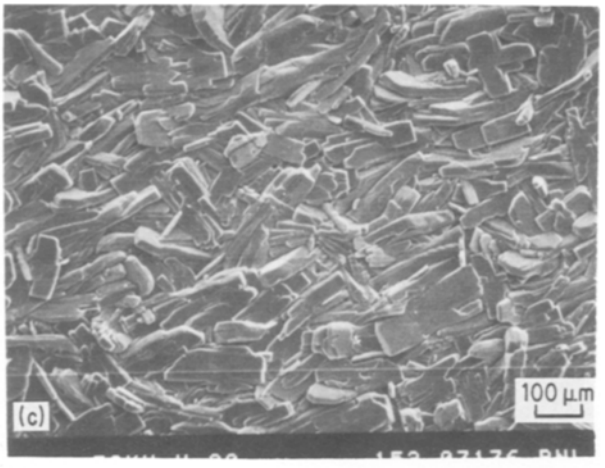

Figure 2 Alteration in Zn · Ph crystal size by polyelectrolyte macromolecules: (a) control, (b) PAA, (c) PSSA.

3. Results and discussion

3.1. Chemisorption

The surface microtopographies of unmodified and 2.0% polyelectrolyte-modified Zn · Ph conversion coatings deposited on the steel surface were studied by low resolution scanning electron microscopy (SEM). Typical micrographs are shown in Figs 2 and 3. The images for both the unmodified and modified Zn · Ph crystalline films, made after immersion of the steel in the zinc phosphating solution for 20 min, reveal interlocking and dense agglomerates of rectangular-like crystals completely covering the substrate surface. The only microscopically discernible difference in the morphology of unmodified and modified crystals is a variation in size of the randomly growing crystals. Fig. 2 shows that the crystal size of Zn · Ph converted by the PAA and PSSA phosphating solutions is notably smaller than that of the unmodified Zn · Ph. A smaller sized crystal was also precipitated when PIA macromolecules were included in the phosphating solution (not shown). There were no such alterations in the crystal dimensions of PAMSA-, PAM-, and PVP-modified Zn · Ph surfaces (Fig. 3). As reported earlier [1], the decreasing crystal size is believed to be

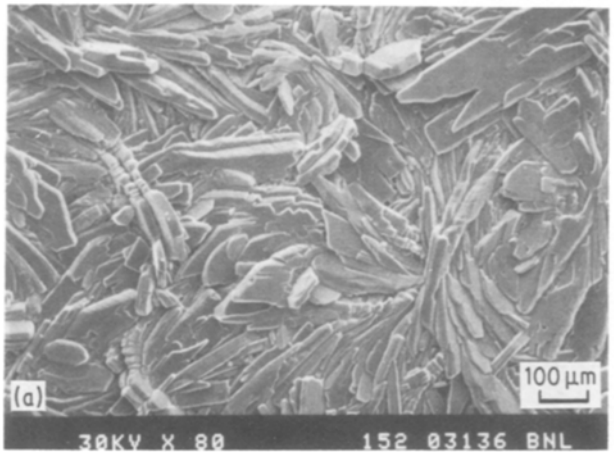

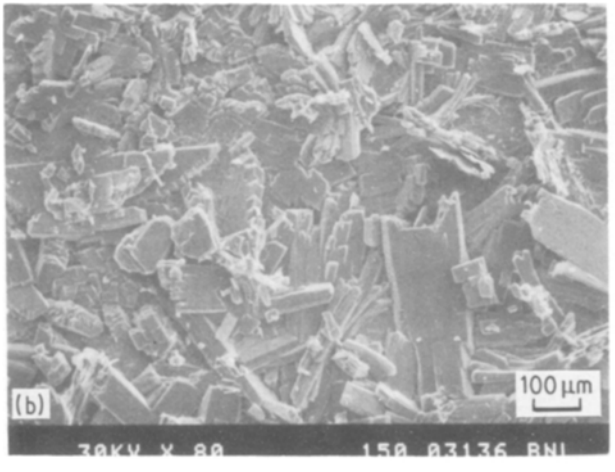

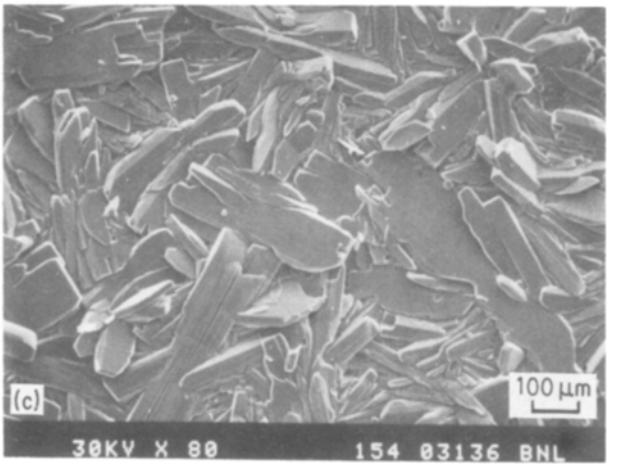

Figure 3 Photomicrographs of (a) PAMSA-, (b) PAM- and (c) PVP-modified Zn · Ph crystal surfaces which suggest that no significant changes in the crystal size occur.

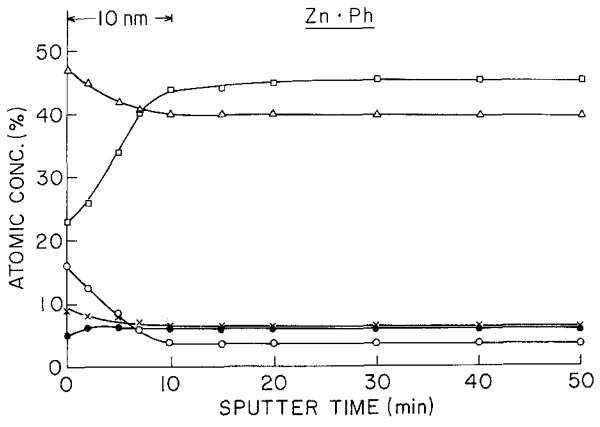

Figure 4 Auger depth profiles for an unmodified Zn · Ph conversion layer: (○) carbon, (●) iron (△) oxygen, (×) phosphorus, (□) zinc.

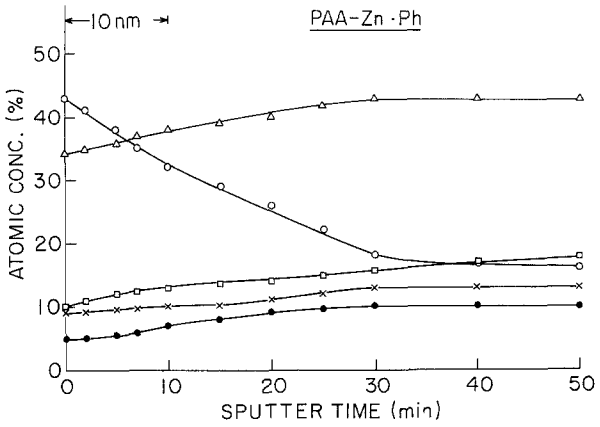

Figure 6 Auger depth profiles for a PAA-chemisorbed Zn · Ph layer system: (○) carbon, (●) iron, (△) oxygen, (×) phosphorus, (□) zinc.

due primarily to segmental chemisorption to the precipitated crystal surfaces of functional electrolyte groups such as carboxylic acid (–COOH) and sulphonic acid ($-SO_3H$).

The magnitude of the chemisorption of organic macromolecules on Zn · Ph crystal faces was identified by studying the depth–composition profile in the conversion layers, using AES in conjunction with argon ion sputter-etching. The sputter rate for the depth profiling was $\sim 1.0\,nm\,min^{-1}$. The profile obtained in ~ 50 min using simultaneous sputtering and analysis permits a rapid identification of layer constituents and structure. The thickness of all of the crystals deposited on the samples tested ranged from ~ 40 to $\sim 10\,\mu m$.

Figs 4 to 9 depict the changes in atomic concentration with sputter time for the unmodified, PIA-, PAA-, PSSA-, PAM- and PAMSA-modified Zn · Ph layers, respectively. In the unmodified Zn · Ph samples (Fig. 4), the approximate concentrations of the elements occupying the outermost surface sites were 48% O, 23% Zn, 16% C, 9% P and 4% Fe. The signal intensity for oxygen, the major component at the surface sites, was gradually reduced as the sputtering time was increased until the concentration stabilized at a value of ~40% after ~10 min. Similar trends were observed for the carbon and phosphorus concentrations, but the zinc and iron atom concentrations initially increased with sputtering time and then levelled off at a depth of ~10 nm. This seems to demonstrate the presence of a high-quality and less contaminated zinc phosphate dihydrate, $Zn_3(PO_4)_2 \cdot 2H_2O$, as a major conversion phase in conjunction with phosphophyllite, $Zn_2Fe(PO_4)_2 \cdot 4H_2O$, and iron phosphate, $Fe(H_2PO_4)_2$, as minor phases at depths greater than 10 nm. The presence of surface carbon is due to the carbonates resulting from the adsorption of atmospheric carbon dioxide by residual hydroxide in the crystal. The constant value for carbon of ~4.2% at depths greater than 10 nm may be associated with contamination by carbon dissociated from the substrate during the conversion reaction processes.

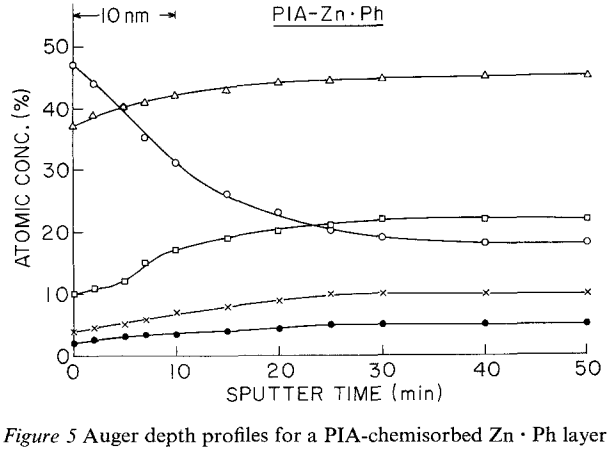

Figure 5 Auger depth profiles for a PIA-chemisorbed Zn · Ph layer system: (○) carbon, (●) iron, (△) oxygen, (×) phosphorus, (□) zinc.

The AES depth profile for PIA-modified Zn · Ph film (Fig. 5) shows that carbon and oxygen were the predominant elements at depths up to ~5 nm from the surface. These reveal the presence of the PIA polymer and carbonaceous species. The carbon content slowly decreased with elapsed sputter time until it levelled off at ~18% at a depth of ~30 nm. Of particular interest was the constant value of carbon reached after a sputtering time of 30 min, that was much higher than the value of contaminated carbon in unmodified Zn · Ph layers. Therefore, even though the PIA–Zn · Ph composite layer contains a certain amount of carbon contaminant, it appears that the carbon element existing at depths greater than 30 nm is due mainly to the PIA macromolecules chemisorbed on the crystal faces throughout the conversion layers. The profiles for other elements such as oxygen, zinc, phosphorus and iron indicate that their concentrations increase monotonically within the first ~30 nm depth and then stabilize. This depth corresponds to the depth at which the carbon stabilized.

Figs 6 and 7 show that the variation in atomic concentration obtained from the PAA- and PSS-modified Zn · Ph conversion surfaces were quite similar to those obtained from the PIA–Zn · Ph composites. Accordingly, the profiling structure of Zn · Ph layers modified with functional polyelectrolytes such as PIA, PAA, and PSSA can be interpreted as follows: (i) highly concentrated polyelectrolyte macromolecules exist throughout the first ~5 nm of the layer, (ii) poorly crystallized zinc and iron phosphate formations caused by chemisorption of the abundant polyelectrolyte are present at depths ranging from 5 to 30 nm, and (iii) there is a well-crystallized phosphate phase in the presence of a small amount of

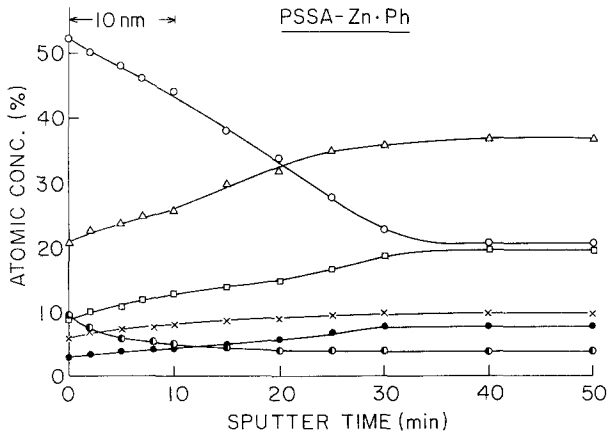

Figure 7 Auger depth profiles for a PSSA-chemisorbed Zn · Ph layer system: (○) carbon, (●) iron, (△) oxygen, (×) phosphorus, (□) zinc.

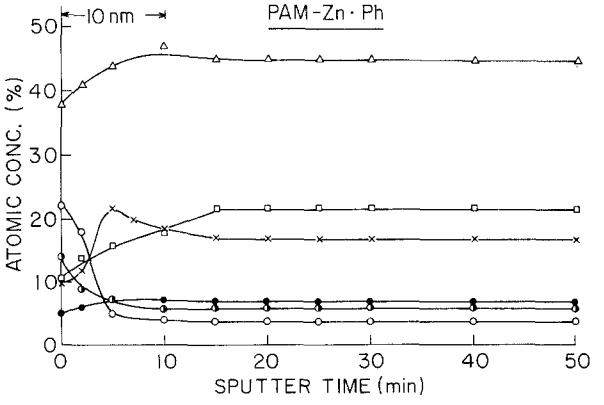

Figure 8 Auger depth profiles for a Zn · Ph layer system modified with a water-soluble PAM macromolecule: (○) carbon, (●) iron, (◑) nitrogen, (△) oxygen, (×) phosphorus, (□) zinc.

polyelectrolyte at depths greater than 30 nm below the surface.

In contrast, the depth–composition profile of the PAM–Zn · Ph composite illustrates quite different features (Fig. 8). The major difference is the carbon atom profile, in which the carbon concentration at the outermost surface sites is considerably lower than that of the oxygen atom. Furthermore, the carbon concentration is conspicuously reduced with increased sputter time within the first five minutes, but subsequently levels off at a depth of ~ 10 nm. This concentrations, of ~ 4.5%, is 25% less than that measured in the PIA–Zn · Ph systems, and is almost equal to that found in unmodified Zn · Ph layers. Therefore, it can be deduced that PAM, which is a water-soluble macromolecule, does not strongly chemisorb on the superficial and internal crystal faces. The ~ 4.5% carbon concentration at depths greater than 10 nm is more likely to be associated with the carbon-contaminated Zn · Ph rather than resulting from chemisorbed organic macromolecules. Since nitrogen can be associated with the presence of pendant NH_2 groups in PAM molecules, this conclusion is supported by the existence of an exiguous amount of nitrogen atoms at depths greater than 10 nm.

Results similar to those for the PAM–Zn · Ph systems were obtained from an AES study of Zn · Ph modified with PVP, another water-soluble macromolecule. These profiles are not included in this paper.

On the other hand, PAMSA macromolecules having two pendant groups, electrolyte COOH and non-electrolyte NH_2 groups, combined to the same backbone carbon atom, can be categorized as semi-polyelectrolyte macromolecules. The resulting profile for the semi-polyelectrolyte-modified Zn · Ph system is depicted in Fig. 9. When compared to those for the PIA– and PAM–Zn · Ph systems, the profiles for oxygen, zinc, phosphorus and iron atoms which represent the conversion crystal formations, exhibit unusual variations in concentration as a function of sputter time. For example, the signal intensities for oxygen and phosphorus atoms slowly increase during the first ~ 5 min sputter time, and subsequently decrease with time. On the other hand, the intensities of the zinc and iron signals progressively grow over the depth range from 0 to 50 nm. The reason for the uncommon features of the profile of these elements is not clear. The carbon depth profile, which relates directly to the presence of PAMSA macromolecules, is very similar to that for the PAM–Zn · Ph system. Therefore, a semi-electrolyte macromolecule appears to be less susceptible to the chemisorbing activity of the crystal faces.

In conjunction with the results from the SEM surface survey, it was found that the presence of functional carboxylic acid (–COOH) and sulphonic acid ($-SO_3H$) pendant groups in the polyelectrolytes act significantly to suppress crystal growth. This is because of the

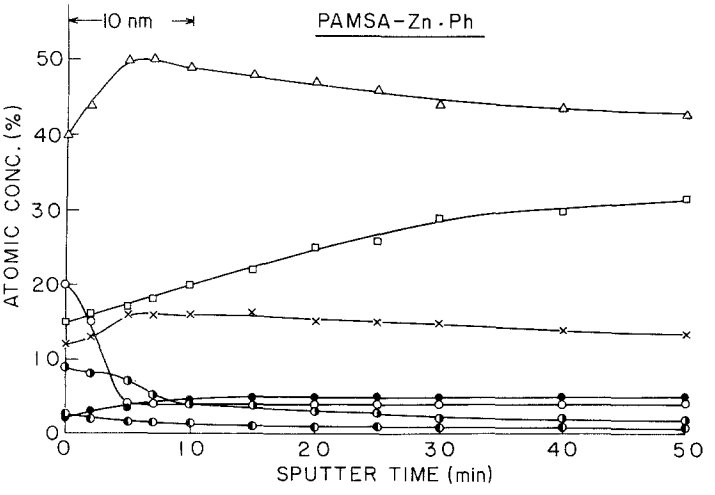

Figure 9 Auger depth profiles for a semi-polyelectrolyte PAMSA–Zn · Ph composite layer: (○) carbon, (●) iron, (◑) nitrogen, (△) oxygen, (×) phosphorus, (◐) sulphur, (□) zinc.

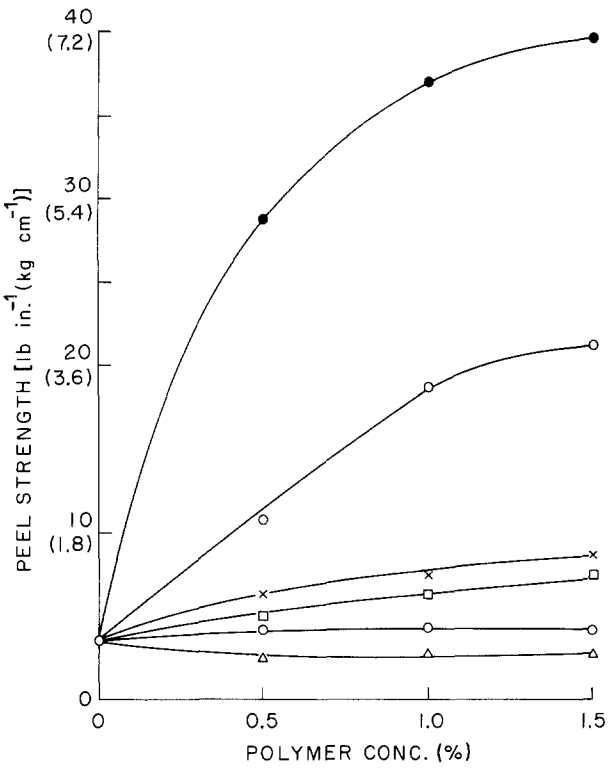

Figure 10 Changes in the 180°-peel strength at PU-to-modified Zn · Ph joints as a function of polyelectrolyte and non-polyelectrolyte macromolecule concentration: (●) PAA, (○) PIA, (×) PSSA, (□) PAMSA, (○) PVP, (△) PAM.

strong chemisorption behaviour of these functional groups on the precipitated crystal faces. In contrast, the magnitude in chemisorbing ability of the amine groups such as $-NH_2$ and $>NH$ is apparently very small.

3.2. Adhesion

The presence of functional organic groups at the outermost surface sites of the conversion coatings serves to promote the adhesive force between the organic polymer topcoat and the crystal precoat. Therefore, the adhesive ability of the polymer–Zn · Ph composite surface was evaluated from the 180°-peel strength of PU topcoat films overlaid on the composite surfaces. In Fig. 10, test results are given that show the variations in peel strength at PU-to-PAA, PSSA, PAMSA, PVP, and PAM-modified and unmodified Zn · Ph interfacial joints. The degree of improvement in adhesive bonds at PU-modified Zn · Ph interfaces appears to depend mainly on the species of the functional groups existing at the surface sites of the Zn · Ph. The PU/PAA and PIA/Zn · Ph joint systems exhibited a great enhancement of peel strength as the concentration of these polyelectrolytes was increased.

In this series, the highest strength value of 7.1 kg cm^{-1} was attained at the adhesive joint between the PU and the 1.5% PAA–Zn · Ph composite. This superior bond force corresponds to an improvement of 11 times over that measured for the PU-to-unmodified Zn · Ph joints. The intrinsic adhesion observed at PU-to-single Zn · Ph joints is attributed to a mechanical interlocking bond that anchors the polymer as a result of the penetration of PU liquid resin into the open spaces and surroundings of the rectangular-like Zn · Ph crystals. The PIA–Zn · Ph composites also displayed a highly reactive surface, although the maximum peel strength was only ~ 50% of that from the PAA–Zn · Ph. The modification of Zn · Ph by PSSA and PAMSA macromolecules resulted in considerably smaller increases in peel strength. In contrast, the interfacial bond strengths for the surfaces of PVP– and PAM–Zn · Ph composite systems were not enhanced by the addition of these macromolecules.

It is useful to assess the interfacial bond mechanism responsible for the great enhancement in polymer–polymer adhesion. To gain this information, specular reflectance IR analyses were made. The samples were prepared by spin-casting the initiated PU resin on to polyelectrolyte-coated and non-polyelectrolyte-coated aluminium mirrors at 4000 r.p.m. The PU film with ~ 200 nm thickness overlaid on the films was then cured in a vacuum oven for 1 h at 150° C. The resultant IR spectra, shown in Fig. 11, were recorded in the frequency range 1900 to 1400 cm^{-1}. The spectrum from the PU-coated aluminium mirror in the absence of polyelectrolyte exhibited absorption bands at about 1715 and 1590 cm^{-1}. These indicate the C=O and the –NH groups in the amide, respectively. Interestingly, spectra obtained from samples having a PIA layer showed the formation of a new band at 1630 cm^{-1} which can be assigned to unsaturated amine, –C=N–, groups. Although not shown, the intensity of this new peak rises conspicuously as the PIA concentration is increased, whereas that of saturated amine at 1590 cm^{-1} tends to decrease. The relative extent of structural transformation from the saturated to unsaturated amine groups is directly related to the intensity of the absorption band or the absorbance at the above two frequencies. This fact proves that amide groups in PU polymer adjacent to the PIA macrolecules can form chemical bonds with the carbonyl of PIA. This interfacial chemical reaction of saturated amine with C=O induces the formation of the unsaturated amines in PU molecules.

An IR spectrum quite similar to that for the PU/PIA interface was obtained for the PU/PAA boundary regions. Therefore, it is believed that the chemical intermolecular reaction is a very important mechanism which greatly enhances the adhesive strength between PU and PAA or PIA having a functional carboxylic acid side group. On the other hand, no obvious signs of chemical intermolecular reactions were identified on the IR spectra at the interfaces of PU/PSSA, PU/PAM and PU/PVP joints. The spectra do not show the growth of any new bands nor any marked shifting of frequencies in the range 1900 to 1400 cm^{-1}. Thus, the reason for the slight increase in peel strength of the PSSA-modified system may be the result of interdiffusion of PU molecules in the absence of strong chemical interactions. This interfacial reaction mechanism is more likely to be of a physical nature.

3.3. Corrosion control

To gain information on the effectiveness of the Zn · Ph and PAA macromolecule-chemisorbed Zn · Ph

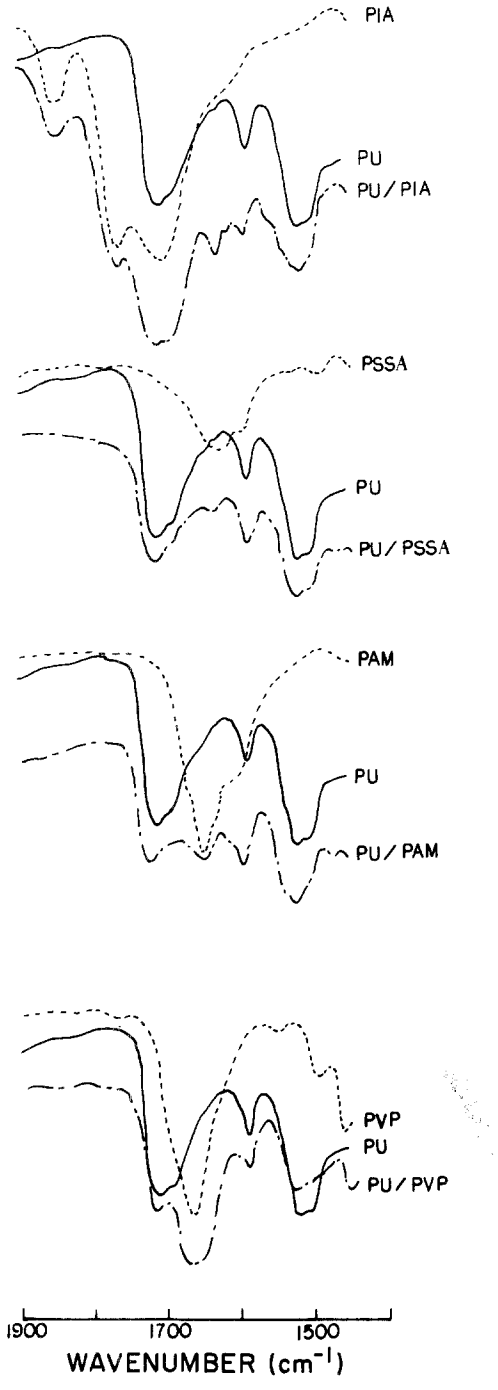

Figure 11 Specular reflectance IR spectra at the interfaces of PU with PIA, PSSA, PAM, and PVP.

conversion coatings as protective layers against corrosion for cold-rolled steel, we examined the electrochemical polarization behaviour of the steel coated with Zn · Ph and PAA–Zn · Ph conversion films. The tests were conducted in a de-aerated 0.5 M NaCl solution at 25° C. Fig. 12 shows typical polarization curves of log (current density) against potential for a plain steel (blank), Zn · Ph-, and modified Zn · Ph-coated steels. The shape of the curves presents the transition from cathodic polarization at an onset of the most negative potential to the anodic polarization curves at an end of lower negative potential. The potential axis at the transition point from cathodic to anodic curves is normalized as the corrosion potential. The important features in a comparison of the cathodic polarization curves from Zn · Ph-coated and uncoated steel specimens are: (i) in the vicinity of the corrosion potential the relative current density of the blank was considerably reduced (approximately by one order of magnitude) by the overlaid Zn · Ph conversion coating, (ii) the short-term steady-state current value for the Zn · Ph specimens was significantly less than that for the blank in the potential region between -1.1 and -1.0 V, thereby suggesting that the evolution of hydrogen is greatly inhibited on Zn · Ph-coated steels, and (iii) a large reduction in corrosion potential to less negative potentials was achieved with the Zn · Ph specimens. It is concluded that the rate of corrosion of steel in a de-aerated NaCl solution is significantly reduced by the presence of the Zn · Ph.

On the other hand, the differences between the curves (Fig. 12) for the PAA-modified Zn · Ph and the unmodified Zn · Ph specimens are: (i) the cathodic peak at -1.09 V grows with increased PAA concentration, (ii) the current density of Zn · Ph at the corrosion potential is reduced by incorporating PAA macromolecules, and (iii) the addition of PAA to Zn · Ph greatly reduces the current density in the anodic potential range from -0.3 to -0.2 V. The cathodic peak at -1.09 V (Result (i) above) may be attributed to the presence of a less stable PAA complex film at the outermost surface sites. This unstable layer may be associated with the hydrolytic transformation of PAA from a solid to a gel state. A possible interpretation for the second result is that the presence of PAA macromolecules chemisorbed on the Zn · Ph crystal faces produces a less effective catalyst for the cathodic reaction at a temperature of 25° C. The third result suggests that a more readily passivated surface of Zn · Ph can be formed by PAA. Therefore, the PAA macromolecules appear to be an effective admixture to further enhance the corrosion resistance of Zn · Ph itself at 25° C.

The electrochemical corrosion studies were extended to explore how the conversion products precipitated on to the steel surfaces during the induction periods for well-crystallized Zn · Ph formation inhibit the corrosion of the steels. The protective ability of the

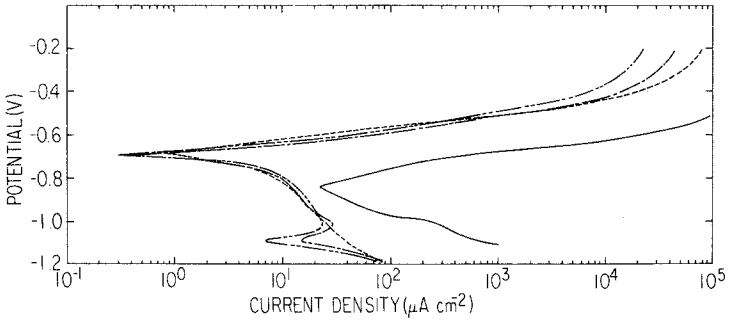

Figure 12 Polarization curves (voltage against saturated calomel electrode) for untreated Zn · Ph- and PAA–Zn · Ph-coated steels immersed in a 0.5 M NaCl solution: (——) blank, (– – –) Zn · Ph, (–·–) 2.0% PAA–Zn · Ph, (–··–) 4.0% PAA–Zn · Ph.

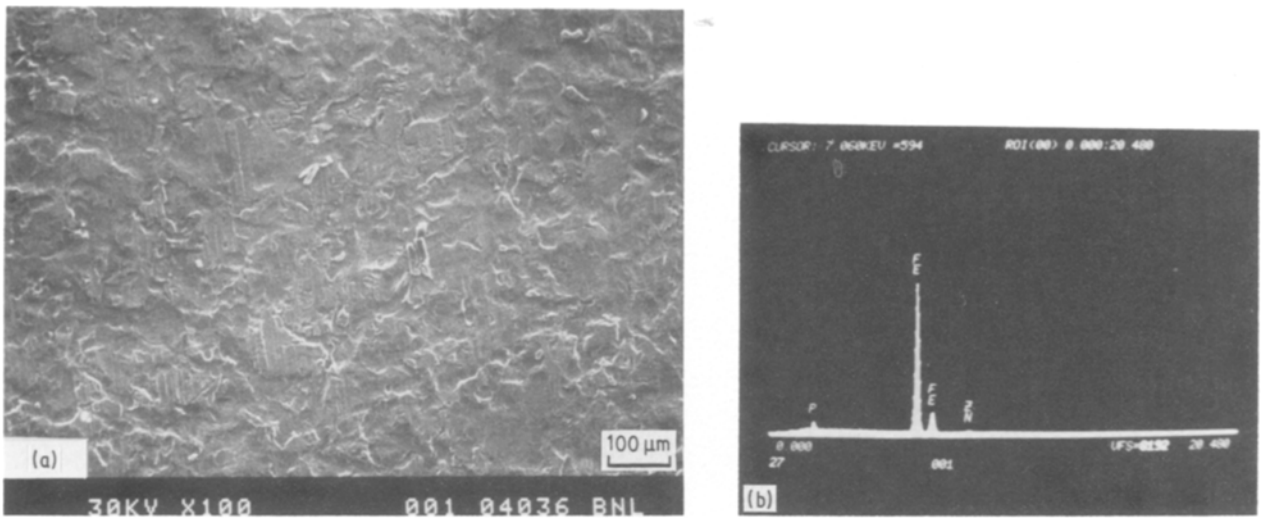

Figure 13 (a) SEM micrograph and (b) EDX of steel surface after immersion in conversion solution at 80° C for 1 min.

conversion layers formed at a certain stage of deposition was estimated on the basis of the current density peaks ($\mu A\,cm^{-2}$). Conversion films were prepared by immersing the steel in a 2.0% PAA-dissolved zinc phosphating solution at 80° C for 1, 3, 5, 10, 15 and 20 min. Their surface morphologies and chemical elements were studied by a combination of SEM and energy-dispersive X-ray spectrometry (EDX) techniques. EDX coupled with SEM has a high potential for the analysis of phases which exist at solid composite material subsurfaces. This feature can greatly enhance the results, as well as facilitating the interpretation of SEM images. These characterizations were made prior to conducting the polarization measurements in a de-aerated 0.5 M NaCl solution at 25° C.

Fig. 13 represents SEM microprobe and EDX elemental analysis of the steel surfaces after immersion in the phosphating solution at 80° C for 1 min. As expected, the SEM image for the surface treated for such a short period revealed a rough texture, and identical crystal formations could not be seen. The EDX spectrum for this surface is also shown in Fig. 13. Iron is the predominant element, which is

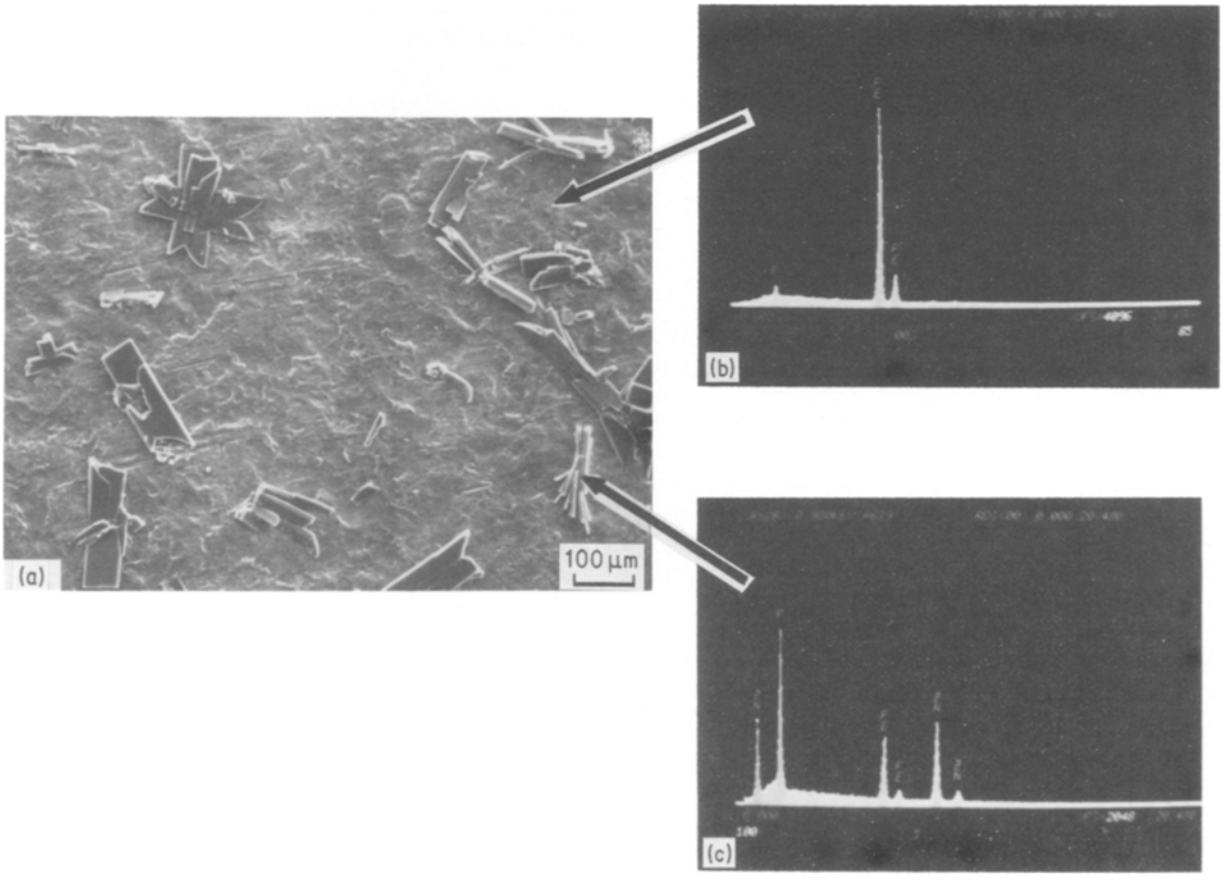

Figure 14 (a) SEM micrograph and (b, c) EDX of conversion crystals precipitated irregularly on iron phosphate layer after treatment for 3 min.

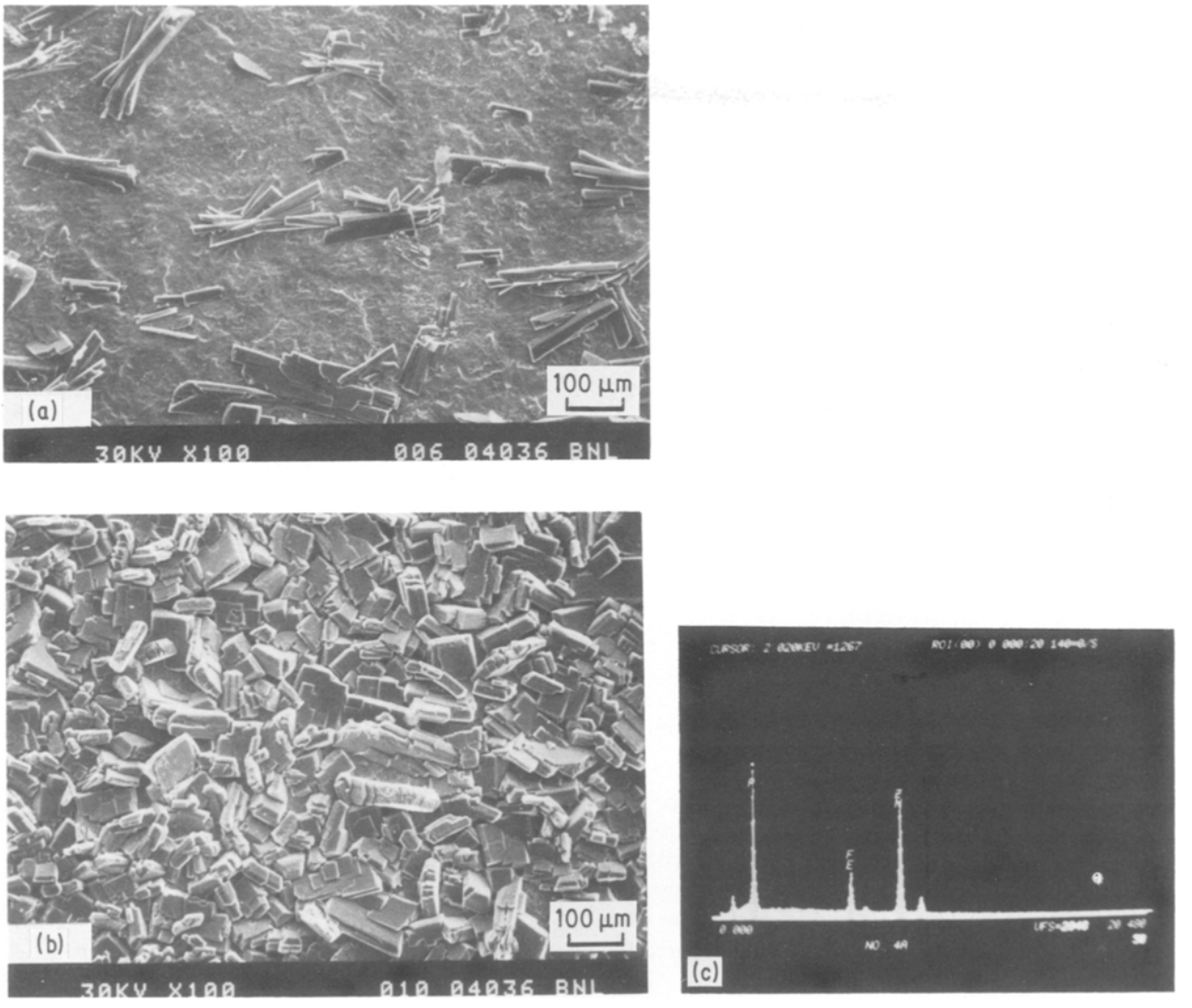

Figure 15 SEM micrographs for (a) 5 and (b) 10 min treated surfaces; (c) EDX for (b).

represented by the highest peak intensity. Other elements present, but with lower peak intensities, are phosphorus and zinc. However, the signal intensity for the zinc atom is considerably weaker than that for the phosphorus atom. The notable peaks for iron and phosphorus atoms suggest that the conversion product formed on the steel surface at the early stages of the treatment is associated with a thin layer of iron-rich phosphate compounds.

The micrograph in Fig. 14 shows that the scattering precipitation of rectangular-like embryo crystals on the iron phosphate layers seems to commence between 1 and 3 min of treatment. The EDX spectrum for this crystal, also shown in Fig. 14, reveals that the dominant element is phosphorus, instead of iron which was dominant in the iron phosphates produced at 1 min conversion times. Further, the peak intensity for iron is almost equal to that of zinc. Thereofre, the embryo crystals are composed of a formation of zinc iron phosphate hydrate, in terms of phosphophyllite, as a major conversion product, and zinc phosphate hydrate as a minor phase.

Extending the treatment to 5 min results in the further occupation of the open iron phosphate layer surface by the embryo crystals (Fig. 15). After a 10 min treatment, the available iron phosphate surfaces seem to be completely covered with the crystalline conversion material (also shown in Fig. 15). As indicated by the accompanying analysis, the crystals covered on the steel substrates apparently contain significant amounts of zinc. Although its concentration is somewhat less than that of phosphorus, it is greater than that of iron. It is believed, therefore, that the well-formed zinc-rich phosphate crystal is primarily a zinc phosphate hydrate compound.

Information was obtained relating to the morphological transformation of the conversion layers with the corrosion resistance of the steel. In this work, current density peaks ($\mu A\,cm^{-2}$) were determined for 2% PAA–Zn · Ph treated steels as a function of conversion times up to 20 min from polarization curves recorded in de-aerated 0.5 M NaCl solutions at 25° C. These values were plotted against the elapsed conversion times, and the results are given in Fig. 16. The data indicate that the peak values decrease rapidly within the first minute of treatment, and then slowly decline with extended time. The value of $\sim 1.9\,\mu A\,cm^{-2}$ for 1 min-treated samples corresponds to an approximately one order of magnitude reduction from that of the untreated steel samples. For samples treated for 20 min, the current peak was $\sim 0.42\,\mu A\,cm^{-2}$.

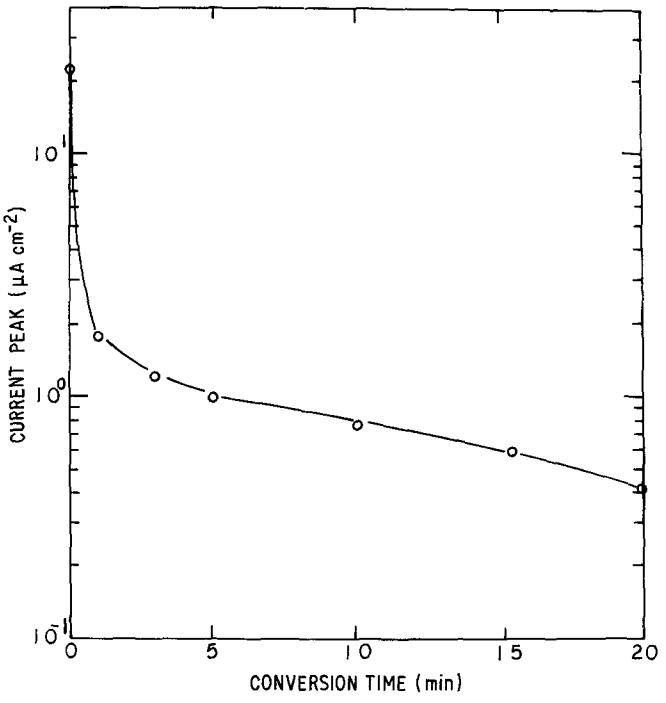

Figure 16 Current density peak against conversion time for steel treated with 2.0% PAA-modified Zn · Ph.

4. Conclusions

The following generalizations can be drawn from our results.

1. The suppression and controllability of the crystal growth of Zn · Ph conversion coatings precipitated on high-strength cold-rolled steels depends primarily on the internal diffusion and segmental chemisorption of polyelectrolytes having functional carboxylic acid and sulphonic acid pendant groups on the embryonic crystal faces.

2. The magnitude of susceptibility of pendant amine groups to chemisorption on crystal growth sites is very small.

3. Interfacial chemical reactions between the amide groups in the polyurethane and carboxylic acid groups existing at the outermost surface sites of PAA and PIA-modified Zn · Ph in the Zn · Ph-to-polymer adhesive joint systems play a key role in promoting adhesive strength.

4. Comparisons between electrochemical polarization curves for untreated steel and Zn · Ph-deposited steel indicate that the corrosion rate in a de-aerated NaCl solution was reduced considerably by the presence of highly dense Zn · Ph crystal arrays derived from a zinc orthophosphate dihydrate-based phosphate solution.

5. The presence of polyelectrolyte macromolecules in the precipitated crystal layers acts to further enhance the corrosion resistance at 25° C of Zn · Ph itself.

6. The major conversion product in the well-precipitated phases was identified as a zinc-rich phosphate hydrate. This is responsible for the corrosion-inhibiting ability of the conversion layers, whereas iron phosphate and iron-rich zinc phosphate hydrate layers which are produced at the beginning of the phosphating treatment have lesser protective effects.

Acknowledgements

This work was performed under the auspices of the US Department of Energy, Washington, DC under Contract No. DE-AC02-76CH00016, and supported by the US Army Research Office Program MIPR-ARO-112-86.

References

1. T. SUGAMA, L. E. KUKACKA, N. CARCIELLO and J. B. WARREN, *J. Mater. Sci.* in press.
2. *Idem, J. Appl. Polym.* **30** (1985) 4357.
3. *Idem, ibid.* **32** (1986) 3469.
4. T. SUGAMA and L. E. KUKACKA, in Proceedings of Tri-Service Corrosion Conference, Orlando, Florida, 1985.
5. R. A. IEZZI and H. LEIDHEISER Jr, *Corrosion* **37** (1981) 28.
6. R. P. WENZ, in "Organic Coatings Science and Technology", Vol. 6, edited by G. D. Parfitt and A. V. Patsis (Dekker, New York, 1984).
7. D. A. JONES and N. R. NAIR, *Corrosion* **41** (1985) 357.

Received 17 December 1986
and accepted 18 February 1987